concentrations from orbit under the assumption of an infinitely deep homogeneous chemistry, when the major-element composition is simultaneously determined using a gamma ray detector [7,8]. Newer calculations reported here show that interpretation of these data can be in error if the hydrogen content of the near-surface regolith is not homogeneous.

Hydrogen is notable for its high efficiency in moderating cosmic-ray-induced fast neutrons to thermal energies. The ratio of thermal to epithermal neutrons (those in the process of slowing) is a very strong function of the hydrogen content. In order to get high precision at low H concentration, however, the abundances of elements that strongly absorb thermal neutrons such as, e.g., Ti, Fe, Sm, and Gd, also need to be determined.

Recent calculations [7,8] showed that a determination of the hydrogen content down to levels of 10 ppm from orbit requires only a 1% statistical precision. However, interpretation of these data is subject to systematic uncertainties that may be larger than the 1% level, depending on the nature and magnitude of H abundance variations as a function of depth. Basically, the reduced mean-scattering path of thermal neutrons caused by the presence of H tends to concentrate neutrons from surrounding material into the high-hydrogen-content side of abundance-changing interfaces. For example, comparison of a lunar meteoritic chemistry loaded uniformly with 100 ppm of hydrogen down to 200 g/cm^2 below the surface, and then with 10 ppm H to the 900 g/cm^2 level, with the same chemistry loaded with 100 or 10 ppm H uniformly down to the 900 g/cm^2 level, shows about 2% variation in subsurface gamma ray production rates (and hence in thermal neutron number density).

Instrumentation: The neutron detection is made with two identical ^{3}He gas proportional counters, one being bare and the other being wrapped in Cd. The bare detector is sensitive to both thermal and epithermal neutrons, whereas the one wrapped in Cd is sensitive only to epithermal neutrons because Cd is a strong absorber of thermal neutrons. The abundances of the strong neutron absorbers in the soil will be made with a simple scintillator gamma ray spectrometer. Although this type of detector does not offer the high sensitivity of cooled semiconductor detectors, they are more than adequate for determination of the abundances of Fe and Ti, the principal neutron absorbers on the Moon. Samarium and Gd are not easily detected with this approach, but because of our extensive database of lunar rock types, these elements can be estimated easily from the abundances of other elements that will be determined with the GRS, especially K, U, and Th.

Delivery and Support System: The instruments will be delivered to the lunar surface via a penetrator with a separable afterbody. Using the soil penetration equations of [9] and assuming a penetrability comparable to dry silt or clay, a forebody mass of 30 kg, a diameter of 7.5 cm, and an impact velocity of 100 m/s, the forebody will penetrate to a depth of about 10 m while the afterbody will remain partially exposed on the surface to maintain communication with Earth. Reduction in this maximum depth can be readily achieved by reducing the impact speed. Both parts will contain neutron and gamma detectors in order to compare the differences between the surface and deep abundances. The penetrator will be battery operated to provide a life of about one week on the lunar surface.

Conclusions: Calculations of the depth dependence of thermal, epithermal, and fast neutron fluxes and consequent capture gamma ray production rates have shown their utility in determining the depth profile of H at the 10 to 100 ppm sensitivity level. Orbital surveys of these same data are not capable of such a determination. The two techniques therefore complement one another. Whereas orbital surveys can provide comprehensive maps of suspected hydrogen concentrations due to solar wind implantation, a penetrator can provide ground truth for a small selection of sites to allow estimates of the depth dependence of such deposits and consequently an evaluation of the utility of such deposits as a source of resources to support human habitation on the Moon.

References: [1] Wittenburg et al. (1986) *Fusion Tech., 10,* 167. [2] Haskin (1989) *LPSC XX,* 387. [3] Arnold (1975) *Proc. LSC 6th,* 2375. [4] Swindle et al. (1990) *Mining Lunar Soils for ^{3}He,* UA/NASA SERC, Tucson. [5] Morris (1976) *Proc. LSC 7th,* 315. [6] Jordan (1990) In *Space Mining and Manufacturing, VII-38,* UA/NASA SERC, Tucson. [7] Metzger A. E. and Drake D. M. (1991) *JGR, 96,* 449–460. [8] Feldman W. C. et al., *GRL, 18,* 2157–2160. [9] Young C. W. (1972) *Sandia Lab. Rep. SC-DR-72-0523.*

ESTIMATING LUNAR PYROCLASTIC DEPOSIT DEPTH FROM IMAGING RADAR DATA: APPLICATIONS TO LUNAR RESOURCE ASSESSMENT.

B. A. Campbell[1], N. J. Stacy[2], D. B. Campbell[2], S. H. Zisk[1], T. W. Thompson[3], and B. R. Hawke[1], [1]Planetary Geosciences, SOEST, University of Hawaii, Honolulu HI, USA, [2]NAIC, Cornell University, Ithaca NY, USA, [3]Jet Propulsion Laboratory, California Institute of Technology, Pasadena CA, USA.

Introduction: Lunar pyroclastic deposits represent one of the primary anticipated sources of raw materials for future human settlements [1]. These deposits are fine-grained volcanic debris layers produced by explosive volcanism contemporaneous with the early stages of mare infilling [2,3]. There are several large regional pyroclastic units on the Moon (for example, the Aristarchus Plateau, Rima Bode, and Sulpicius Gallus formations), and numerous localized examples, which often occur as dark-halo deposits around endogenic craters (such as in the floor of Alphonsus Crater). Several regional pyroclastic deposits have been studied with spectral reflectance techniques: The Aristarchus Plateau materials were found to be a relatively homogeneous blanket of iron-rich glasses [4,5]. One such deposit was sampled at the Apollo 17 landing site, and was found to have ferrous oxide and titanium dioxide contents of 12% and 5% respectively [6]. While the areal extent of these deposits is relatively well defined from orbital photographs, their depths have been constrained only by a few studies of partially filled impact craters and by imaging radar data [7,1]. In this work, we present a model for radar backscatter from mantled units applicable to both 70-cm and 12.6-cm wavelength radar data. Depth estimates from such radar observations may be useful in planning future utilization of lunar pyroclastic deposits.

Radar Scattering Model: The depth of a pyroclastic layer is estimated based upon the ratio of backscattered power between a mantled region and an area of unmantled terrain assumed to represent the buried substrate. Several conditions are required: (1) Only the depolarized (same-sense circular) echo is modeled, to avoid consideration of large single-scattering facets; (2) there is no volume scattering within the pyroclastic (i.e., there are no inclusions large with respect to the radar wavelength); and (3) the depolarized backscatter originates largely within the regolith substrate, and not at its upper surface. Conditions (2) and (3) are supported by previous studies of the eclipse temperatures

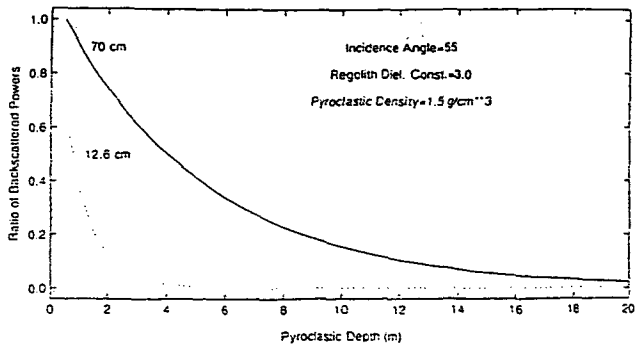

Fig. 1.

of pyroclastic deposits and analysis of 70-cm backscattering from the lunar regolith [8,9].

Input parameters to the model are the radar wavelength, the radar incidence angle, and the dielectric parameters of the pyroclastic layer and the regolith substrate. The model used here permits analysis of a pyroclastic layer with varying density as a function of depth. The electrical properties of an Apollo 17 glass sample [6] as a function of density ρ are used here:

$$\epsilon_r = 2.1^{\rho} \tan \delta = 0.0037\ \rho$$

where ϵ_r is the real dielectric constant and tan δ is the radar loss tangent. The real dielectric constant of the lunar regolith has been measured to be ~3.0, but may vary from mare to highland regions [10]. The incident circularly polarized wave is decomposed into horizontal and vertical polarized components, and the Fresnel transmission coefficients for each interface are calculated. Attenuation within the pyroclastic is assumed to be exp(-2αL), where L is the path length and α is the attenuation coefficient [11]

$$\alpha = k\,(0.5^{*}[(\tan\delta^2 + 1)^{0.5} - 1])^{0.5}$$

where k is the radar wavenumber in the pyroclastic deposit. This expression is solved numerically in our model for the varying density within the lossy medium.

All the scattered radiation within the regolith layer is assumed to be randomly polarized, with some total backscattering efficiency S. In our model, we thus combine the H- and V-polarized components within the regolith, multiply by S, and split the remaining power evenly between the two polarizations for the return trip to the surface. The energy that exits the pyroclastic is assumed to have random phase, but may have an elliptical polarization due to the differing H and V transmission coefficients. The scatter from an unmantled regolith is also calculated, and the two results are combined into a ratio of total mantled/unmantled backscatter. This cancels the S term in both expressions. The ellipticity of the final scattered wave is assumed to be close to unity. The results are plotted as a function of power ratio vs. depth for a given set of electrical and density parameters.

In mathematical terms, the H and V backscattered powers from a mantled region are

$$P_h = 0.25 * S * A^2 * (T_h^{s/p} * T_h^{p/r} + T_v^{s/p} * T_v^{p/r}) * T_h^{r/p} * T_h^{p/s}$$
$$P_v = 0.25 * S * A^2 * (T_h^{s/p} * T_h^{p/r} + T_v^{s/p} * T_v^{p/r}) * T_v^{r/p} * T_v^{p/s}$$

where A is the total attenuation factor, and the T terms refer to H- and V-polarized Fresnel transmission coefficients for the layer interfaces noted in their superscripts; s, p, and r refer to space, pyroclastic, and regolith respectively. The backscattered powers from an unmantled area are

$$Ph = 0.25 * S * (T_h^{s/r} + T_v^{s/r}) * T_h^{r/s}$$
$$Pv = 0.25 * S * (T_h^{s/r} + T_v^{s/r}) * T_v^{r/s}$$

Results: Figure 1 shows an example of this model for an incidence angle of 55°, corresponding to the Earth-based viewing geometry for the Aristarchus Plateau. The pyroclastic density was assumed to be a uniform 1.5 g/cm^3. The regolith real dielectric constant is assumed to be 3.0. Both 70-cm and 12.6-cm radar wavelengths are tested, and it is seen that the shorter wavelength is attenuated much more rapidly in the pyroclastic, as expected. The ratio between average 70-cm returns from the plateau and the mean lunar echo is ~0.30, implying a depth of 6–7 m based on these electrical parameters. This estimate is a lower bound; the actual buried highland terrain is likely much brighter than the Moon-wide average, implying a greater mantle depth.

Tests of the above model show that (1) it is relatively insensitive to variations in incidence angle between 20° and 60°, (2) it is insensitive to regolith dielectric variations from 2.5 to 4.0, (3) the scattered wave ellipticity is >85%, and (4) density variations with depth in the pyroclastic, within the narrow range permitted by realistic values of 1.5–2.0 g/cm^3, are not important unless the changes are very rapid. The value of the density at the upper surface of the layer is probably a satisfactory estimate for the overall density of such shallow deposits.

Conclusions: This technique may permit remote estimates of pyroclastic mantle depths from either Earth-based or lunar-orbital radar systems. A 3-km resolution map of the lunar nearside is available for 70-cm radar wavelength [12], and ongoing work at Arecibo Observatory provides additional data at 12.6-cm wavelength. We anticipate that such studies will be required in the planning stages of a lunar base project for resource assessment.

References: [1] Hawke B. R. et al. (1990) *Proc. LPS, Vol. 21*, 377–389. [2] Head J. W. (1974) *Proc. LSC 5th*, 207–222. [3] Wilson L. and Head J. W. (1981) JGR, 86, 2971–3001. [4] Gaddis L. R. et al. (1985) *Icarus, 61*, 461–489. [5] Lucey P. G. et al. (1986) *Proc. LPSC 16th*, in JGR, 91, D344–D354. [6] Bussey H. E. (1979) *Proc. LPSC 10th*, 2175–2182. [7] Zisk S. H. et al. (1977) *Moon, 17*, 59–99. [8] Moore H. J. et al. (1980) *USGS Prof. Paper 1046-B*. [9] Thompson T. W. and Zisk S. H. (1972) In *Prog. in Aero. and Astro.*, 83–117. [10] Hagfors T. and Evans J. V. (1968) In *Radar Astronomy*, 219–273. [11] Ulaby F. T. et al. (1986) In *Microwave Remote Sensing*, 67. [12] Thompson T. W. (1987) *Earth Moon Planets, 37*, 59–70.

A GROUND-BASED SEARCH FOR LUNAR RESOURCES USING HIGH-RESOLUTION IMAGING IN THE INFRARED.

C. R. Coombs and T. S. McKechnie, POD Associates, Inc., 2309 Renard Place SE, Suite 201, Albuquerque NM 87109, USA.

Introduction: When humans return to the Moon (". . . this time to stay . . ." [1]) lunar resources will play an important role in the successful deployment and maintenance of the lunar base. Previous studies have illustrated the abundance of resource materials available on the surface of the Moon, as well as their ready accessibility [e.g., 2–5]. Particularly worth considering are the lunar regional (2000–30,000 km^2) pyroclastic deposits scattered about the lunar nearside. These 30–50-m-thick deposits are composed